

Nuclear Shell Effects near r-Process Path at N=82 in the Relativistic Hartree-Bogoliubov Theory

Madan M. Sharma and Ameena R. Farhan
 Physics Department, Kuwait University, Kuwait 13060
 (November 1, 2018)

Evolution of the shell structure of nuclei near the neutron drip line is investigated in the Relativistic Hartree-Bogoliubov (RHB) theory. By introducing the vector self-coupling of ω meson in the RHB theory, we reproduce successfully the experimental data on the shell effects about the waiting-point nucleus ^{80}Zn . With this basis, it is shown that the shell effects at $N = 82$ in the inaccessible region of the r-process path remain strong. In contrast, a quenching exhibited by the HFB+SkP approach is shown to be incompatible with the available data. Consequently, the neutrino-driven mechanism of the nucleosynthesis is supported.

PACS numbers: 21.10.Dr, 21.30.Fe, 21.60.-n, 21.60.Jz

A knowledge of shell effects near the drip lines is important to discerning astrophysical scenario of nucleosynthesis [1]. The question whether the shell effects near the drip lines are strong or do quench has become crucial to understanding heavy nucleosynthesis. The $N = 82$ nuclei at r-process path are assumed to play a significant role in providing nuclear abundances about $A \sim 130$. Since nuclei contributing to this peak are extremely neutron-rich and are not accessible experimentally, it has not been possible to ascertain the nature of the shell effects in the vicinity of the neutron drip line. Due to the lack of experimental data, there prevail conflicting view points [2,3] on the strength of the shell effects near the neutron drip line. There exist different scenarios regarding the r-process nuclear abundances such as the one assisted by shell quenching [1], or that of neutrino-driven post-processing [4,5].

In this letter, we examine how the shell effects evolve with isospin in the region of the astrophysically important magic number $N = 82$ near the neutron drip line. Using the experimental data available on the shell effects around the waiting-point nucleus ^{80}Zn ($N = 50$) as a benchmark, we will explore the shell effects near the r-process path in the framework of the Relativistic Hartree-Bogoliubov (RHB) theory with the self-consistent finite-range pairing. We have introduced the vector self-coupling of ω meson in addition to the non-linear scalar coupling of the σ -meson in the RHB theory. The high-precision experimental data about the stability line and a successful description of the ensuing shell effects [6] constitutes our basis to predict the shell effects in the inaccessible region.

The shell effects are known to manifest strongly in terms of the magic numbers. This is demonstrated by a prominent kink about the major magic numbers [7] in the 2-neutron separation energies (S_{2n}) all over the periodic table. This implies that there exist large shell gaps at the magic numbers about the stability line. The spin-orbit interaction is pivotal [8] in creation of the magic num-

bers. In the Relativistic Mean Field (RMF) theory [9] the spin-orbit term arises as a result of the Dirac-Lorentz structure of nucleons. This has shown much usefulness in explaining properties which involve shell effects such as anomalous isotope shifts in stable nuclei [10]. The form of the spin-orbit interaction in the RMF theory has also been found to be advantageous over that in the non-relativistic approach [11].

For nuclei near a drip line, a coupling to the continuum is required. A self-consistent treatment of pairing is also desirable. The framework of RHB theory provides an appropriate tool to include both these features. Thus, in the RHB theory the advantages of a relativistic description of the RMF approach in the Hartree channel are combined with that of a finite-range pairing force.

The RMF Lagrangian which describes the nucleons as Dirac spinors moving in meson fields is given by [9]

$$\begin{aligned} \mathcal{L} = & \bar{\psi} \left(\not{\partial} - g_\omega \not{\omega} - g_\rho \not{\vec{\rho}} \vec{\tau} - \frac{1}{2} e(1 - \tau_3) \not{A} - g_\sigma \sigma - M_N \right) \psi \\ & + \frac{1}{2} \partial_\mu \sigma \partial^\mu \sigma - U(\sigma) - \frac{1}{4} \Omega_{\mu\nu} \Omega^{\mu\nu} + \frac{1}{2} m_\omega^2 \omega_\mu \omega^\mu \quad (1) \\ & + \frac{1}{2} g_4 (\omega_\mu \omega^\mu)^2 - \frac{1}{4} \vec{R}_{\mu\nu} \vec{R}^{\mu\nu} + \frac{1}{2} m_\rho^2 \vec{\rho}_\mu \vec{\rho}^\mu - \frac{1}{4} F_{\mu\nu} F^{\mu\nu} \end{aligned}$$

where M_N is the bare nucleon mass and ψ is its Dirac spinor. In addition, we have the scalar meson (σ), isoscalar vector mesons (ω), isovector vector mesons (ρ) and the photons A^μ , with the masses m_σ , m_ω and m_ρ and the coupling constants g_σ , g_ω , g_ρ , respectively. The field tensors for the vector mesons are given as $\Omega_{\mu\nu} = \partial_\mu \omega_\nu - \partial_\nu \omega_\mu$ and by similar expressions for the ρ -meson and the photon. For a realistic description of nuclear properties a nonlinear self-coupling $U(\sigma) = \frac{1}{2} m_\sigma^2 \sigma^2 + \frac{1}{3} g_2 \sigma^3 + \frac{1}{4} g_3 \sigma^4$ for σ -mesons is taken. We have added the non-linear vector self-coupling of ω -meson [12] as represented by the coupling constant g_4 .

Using Green's function techniques [13] it has been shown in Ref. [14] that a relativistic Hartree-Bogoliubov theory can be implemented using such a Lagrangian.

Neglecting retardation effects one obtains a relativistic Dirac-Hartree-Bogoliubov (RHB) equations

$$\begin{pmatrix} h & \Delta \\ -\Delta^* & -h^* \end{pmatrix} \begin{pmatrix} U \\ V \end{pmatrix}_k = E_k \begin{pmatrix} U \\ V \end{pmatrix}_k, \quad (2)$$

where E_k are quasiparticle energies and the coefficients U_k and V_k are four-dimensional Dirac spinors normalized as

$$\int (U_k^+ U_{k'} + V_k^+ V_{k'}) d^3r = \delta_{kk'}. \quad (3)$$

The average field

$$h = \boldsymbol{\alpha} \mathbf{p} + g_\omega \omega + \beta(M + g_\sigma \sigma) - \lambda \quad (4)$$

contains the chemical potential λ which is adjusted to the proper particle number. The meson fields σ and ω are determined self-consistently from the Klein Gordon equations:

$$\{-\Delta + m_\sigma^2\} \sigma = -g_\sigma \rho_s - g_2 \sigma^2 - g_3 \sigma^3, \quad (5)$$

$$\{-\Delta + m_\omega^2\} \omega = g_\omega \rho_v + g_4 \omega^3, \quad (6)$$

with the scalar density $\rho_s = \sum_k \bar{V}_k V_k$ and the baryon density $\rho_v = \sum_k V_k^+ V_k$. The sum on k runs only over all the particle states in the no-sea approximation. The pairing potential Δ in Eq. (2) is given by

$$\Delta_{ab} = \frac{1}{2} \sum_{cd} V_{abcd}^{pp} k_{cd} \quad (7)$$

The RHB equations (2) are a set of four coupled integro-differential equations for the Dirac spinors $U(r)$ and $V(r)$ which are obtained self-consistently. Here the RHB calculations have been performed by expanding fermionic and bosonic wavefunctions in 20 oscillator shells for a spherical configuration. We have used the force NL-SH [15] with the non-linear scalar self-coupling and the forces NL-SV1 and NL-SV2 with both the scalar and the vector self-couplings. The forces NL-SV1 and NL-SV2 have been developed with a view to soften the high-density equation of state of nuclear matter and are shown to improve the ground-state properties of nuclei [6,16]. For the pairing channel, we have taken the finite-range Gogny force D1S. It is known to represent the pairing properties of a large number of finite nuclei appropriately [17].

In our previous work [6], we started with the shell effects at the stability line, where we examined the role of σ - and ω -meson couplings on the shell effects in Ni and Sn isotopes. It was found that the existing nuclear forces based upon the nonlinear scalar self-coupling of σ -meson exhibit shell effects which were stronger than suggested by the experimental data. In order to remedy this problem, the nonlinear vector self-coupling of ω -meson in the RHB theory was introduced. Consequently, the experimental data on shell effects in nuclei about the stability line were reproduced well [6].

Having established the basis, we consider nuclei about ^{80}Zn ($N = 50$) in the present work. ^{80}Zn is a waiting point nucleus and here the r-process path comes closest to the β -stability. The empirical values on the binding energy of ^{80}Zn and ^{82}Zn are taken from the compilation by Wapstra and Audi [18]. These data provide a unique opportunity to probe the nature of the shell effects away from the stability line.

Results on S_{2n} values for the Zn isotopes are shown in Fig. 1. The kink at $N = 50$ shows that NL-SH (scalar self-coupling only) exhibits shell effects which are much stronger than the experimental data. In comparison, the shell gap with NL-SV2 (both the scalar and vector self-couplings) [6] is reduced as compared to NL-SH. It is, however, still larger than the experimental one. We show in Fig. 1(b) the S_{2n} values obtained with the force NL-SV1 [6]. The slope of the kink shows that the shell gap with NL-SV1 agrees well with the experimental value. Thus, RHB with the force NL-SV1 is able to reproduce the empirical shell effects in the waiting point region. A comparison with the HFB+SkP results [19] shows that the shell effects with SkP are strongly quenched. In contrast, the data show that the shell effects in the waiting point region are much stronger than those predicted by SkP. This is consistent with our earlier conclusion [6] that the shell effects with SkP are quenched strongly already at the stability line. This behaviour is evidently due to its high effective mass $m^* \sim 1$ [19] which suppresses the shell gaps significantly.

In Fig. 1(c) we compare various predictions of the mass formula Extended Thomas-Fermi with Strutinsky Integral (ETF-SI) [20]. It is widely used in the abundance calculations of the r-process nucleosynthesis due to its success in reproducing the binding energies of nuclei over a wide range of the periodic table. It can be seen from the figure that ETF-SI reproduces the shell effects in the waiting point region successfully. However, motivated by the results of HFB+SkP, a phenomenological quenching of the shell effects has recently been introduced [21] in ETF-SI, thus producing a new mass table ETF-SI (Q). The results [Fig. 1(c)] of the quenched (Q) mass formula show that the shell effects are weakened as compared to the experimental data and ETF-SI. We have found several other cases where a good agreement of ETF-SI with the experimental data is deteriorated in going to ETF-SI(Q). Thus, the introduction of the quenching in ETF-SI (Q) seems to be unnecessary notwithstanding the success of ETF-SI.

The RHB results with NL-SV1 in Fig. 1(b) provide a confidence to extend our formalism to explore the inaccessible region of the neutron drip-line about $N = 82$. In order to visualize how the shell effects evolve as one approaches the continuum, we have chosen the isotopic chains of Kr, Sr, Zr and Mo ($Z = 36 - 42$). The S_{2n} values as obtained in RHB with the various forces are shown

in Fig. 2. For a given force, the shell gap at $N = 82$ shows a steady decrease in moving from Mo (a) to Kr (d). Evidently, nuclei become increasingly unbound and a coupling to the continuum arises in going to larger neutron to proton ratios.

The results [Fig. 2] with the non-linear scalar coupling (NL-SH) show a shell gap at $N = 82$, which is largest amongst all the forces. The strong shell effects with NL-SH were also noted for $N = 82$ nuclei near the drip line in ref. [2]. These results were based upon the BCS pairing and the shell effects along the stability line were not taken into account appropriately. This emphasizes the importance of the self-consistent pairing and of the data available on the shell effects in the known region.

With the force NL-SV2 with the vector self-coupling of ω -meson, the shell effects [Fig. 2] are milder as compared to NL-SH for all the chains. This is similar to that observed at the stability line [6] and also in Fig. 1(a). The results [Fig. 2] with our benchmark force NL-SV1 show that the shell gap at $N = 82$ is reduced as compared to NL-SV2. This is again similar to that observed for the Zn isotopes. However, the shell effects with NL-SV1 are still stronger as compared to the HFB+SkP results shown in the figure. This is especially true for Mo and Zr isotopes at $N=82$, where the r-process path is assumed to pass through. The quenching shown by SkP in this region is as expected. As noted earlier HFB+SkP is known to exhibit a strong quenching at the stability line [6] and near the waiting-point nucleus ^{80}Zn as shown in Fig. 1(b) above. In comparison, the RHB approach with NL-SV1 reproduces the shell effects about the stability line [6] as well as in the waiting-point region at $N = 50$.

The shell effects with NL-SV1 become successively weaker (which is true for all the forces) as one moves to nuclei with higher isospin such as ^{120}Sr [Fig. 2(c)] and ^{118}Kr [Fig. 2(d)]. The case of Kr isotopes [Fig. 2(d)] deserves a special mention. Except with NL-SH, all the other forces show a complete washing out of the shell effects. This stems from the fact that for ^{118}Kr , the Fermi energy is very close to the continuum and the nucleus is pushed to the very limit of binding. The binding energy of an additional neutron is close to zero and consequently the shell gap ceases to exist. Thus, any semblance of the shell effects for ^{118}Kr ($N = 82$) is completely lost. Such nuclei at the drip line ($\lambda_n \sim 0$) should be of little interest to the r-process as these nuclei show no binding to an additional neutron. However, as the r-process path passes through $S_n \sim 2 - 4$ MeV, it is seen [Figs. 2(a) and 2(b)] that nuclei which ought to contribute to the r-process show a persistence of stronger shell gaps in contrast to that seen for Kr and Sr. Figures 2(a) and 2(b) show that with NL-SV1 the shell effects for Mo ($Z=42$) and Zr ($Z=40$) nuclei at $N = 82$ are much stronger than with SkP. Shell gaps are expected to be even larger for r-process nuclei with $Z > 42$. Thus, notwithstanding the fact that NL-SV1 is commensurate with the experimen-

tal data available in the waiting point region, it can be concluded that the shell effects about the r-process path remain stronger.

We show in Fig. 3(a) the neutron single-particle levels obtained with NL-SV1 for $N = 80$ nuclei. Our focus is the evolution of the shell gap at $N = 82$ as one approaches the drip line ($\lambda_n \sim 0$). The single-particle levels shown in this figure portray the results of Fig. 2. The Fermi energy (shown by the dashed lines) approaches the continuum as one moves towards a larger neutron to proton ratio. The shell gap ($N = 82$) shows a constant decrease as the last neutrons become more and more unbound in going from Mo to Kr. For ^{118}Kr ($N = 82$) the Fermi energy is close to zero and the shell gap diminishes significantly. However, for nuclei on the r-process path such as Mo and Zr, shell gaps do remain large.

The difference in the response of the various forces near the drip line is illustrated in single-particle levels shown for ^{120}Zr in Fig. 3(b). The shell gap at $N = 82$ is largest with NL-SH and shows a reduction in going to NL-SV1. On the other hand, the shell gap with SkP is reduced significantly as compared to NL-SV1. The reduced shell strength with SkP seems to be generic as discussed above.

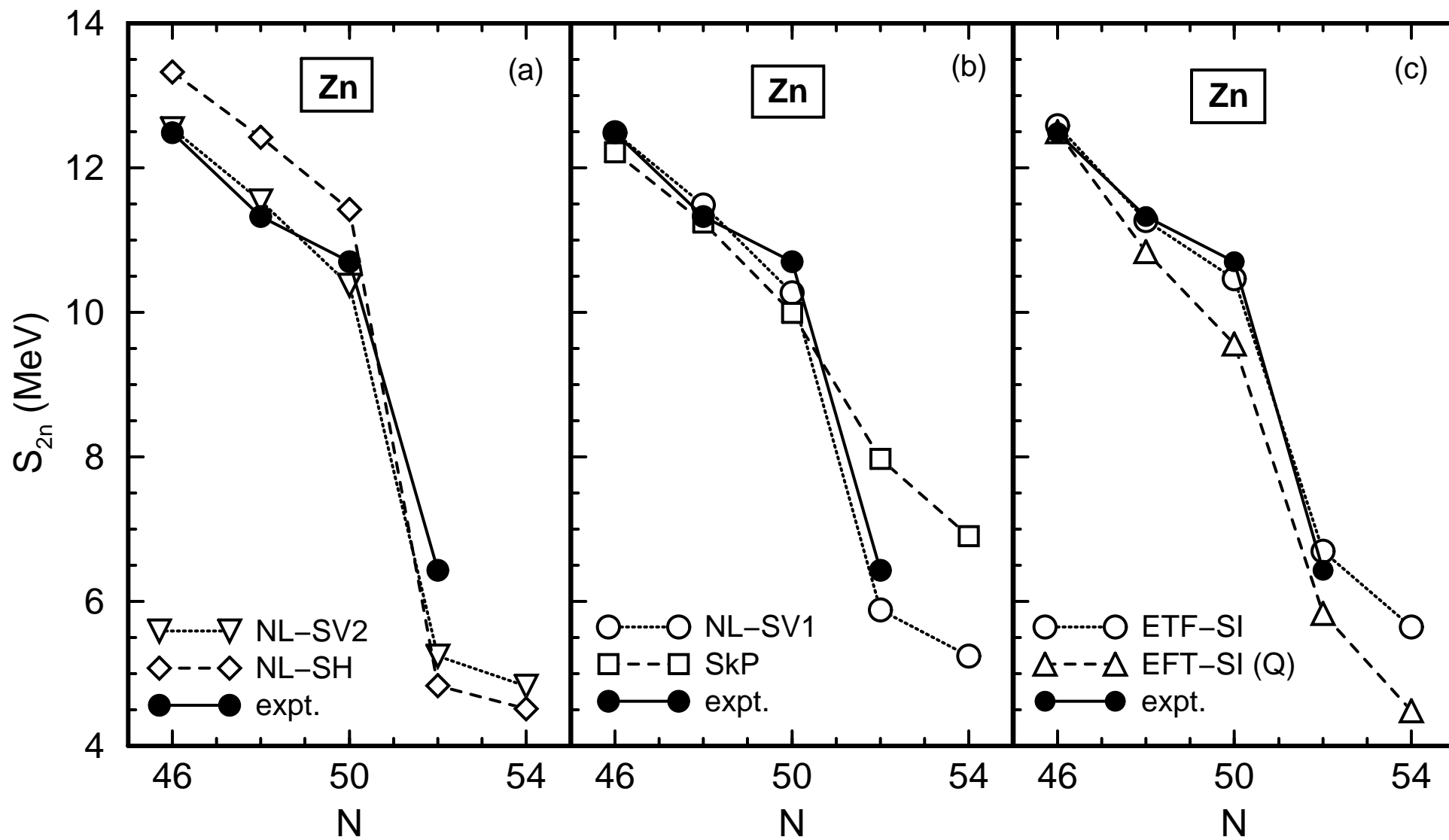
In conclusion, we have reproduced the shell effects in the waiting-point nucleus ^{80}Zn with the vector self-coupling of ω -meson in the RHB theory. Having our working basis established, we show that the shell effects near the r-process path about $N = 82$ remain strong vis-a-vis a quenching exhibited by HFB+SkP. The oft-discussed quenching with SkP is, however, not supported by the available experimental data in the waiting-point region. It is noteworthy that on the basis of the results with SkP, a quenching has been requested for an improved fit to the global r-process abundances [1]. Since SkP fails to reproduce the shell effects at the stability line and in the waiting-point region, an improved fit alone does not necessarily imply a shell quenching near the r-process path. On the other hand, our results on the stronger shell effects at the r-process path are consistent with the point made in refs. [4,5] that neutrino-induced reaction during a core-collapse supernova can be effective in breaking through the waiting-point nuclei and that it is not necessary to invoke a quenching of the shell strength. In view of this, the present results support neutrino-induced reaction as a plausible mechanism of nucleosynthesis of heavy nuclei.

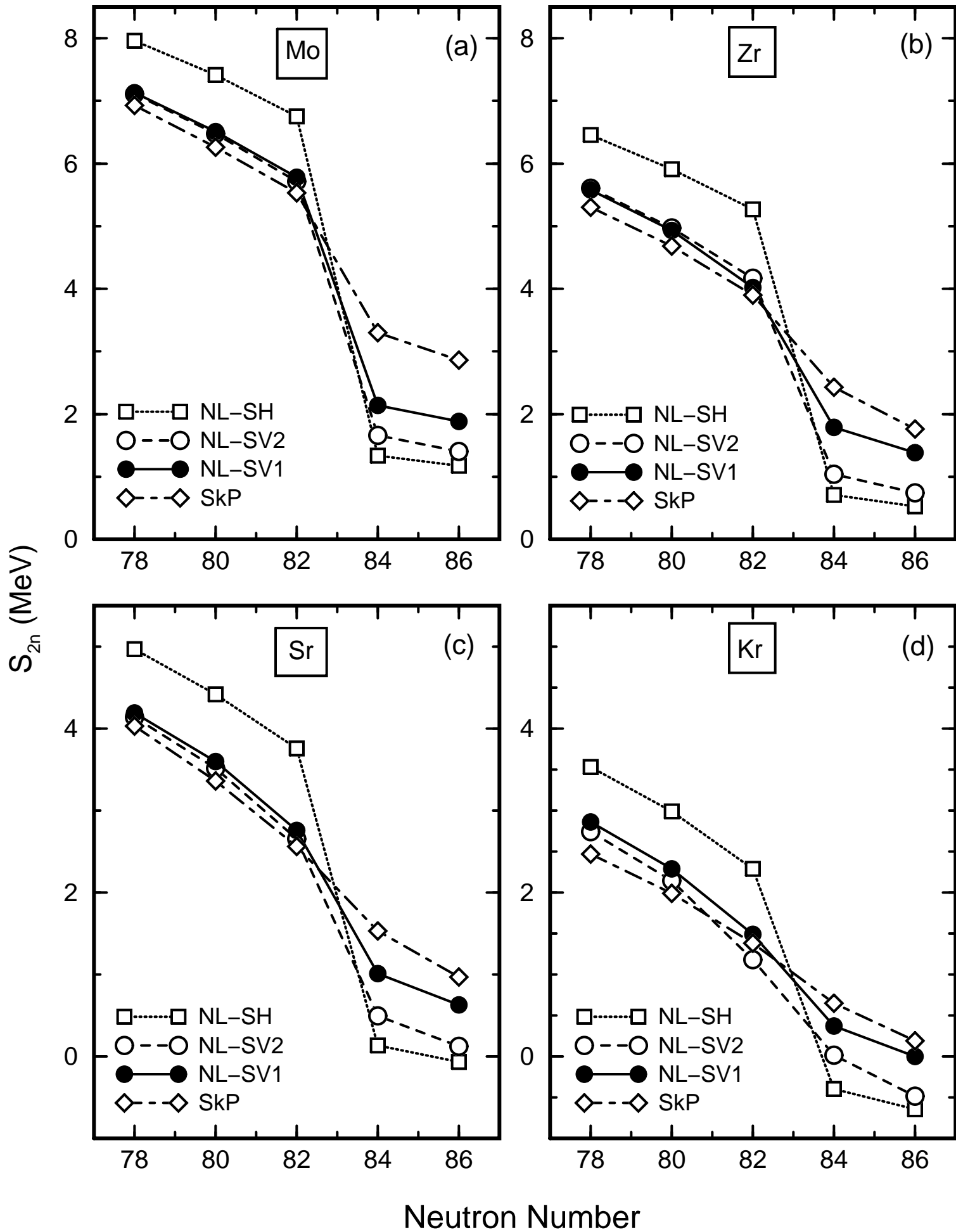
This work is supported by the Research Administration Project No. SP056 of the Kuwait University. We thank Prof. J.M. Pearson for providing us ETF-SI(Q) table before its publication.

- [1] K.-L. Kratz *et al.*, *Astrophys. J.* **403**, 216 (1993).
- [2] M. M. Sharma, G. A. Lalazissis, W. Hillebrandt, and P. Ring, *Phys. Rev. Lett.* **72**, 1431 (1994).
- [3] J. Dobaczewski *et al.*, *Phys. Rev. Lett.* **72**, 981 (1994).
- [4] W. C. Haxton *et al.*, *Phys. Rev. Lett.* **78**, 2694 (1997).
- [5] Y.-Z. Qian *et al.*, *Phys. Rev. C* **55**, 1532 (1997).
- [6] M. M. Sharma, A. R. Farhan and S. Mythili, *Phys. Rev. C* **61** ??? (2000).
- [7] C. Borcea *et al.*, *Nucl. Phys. A* **565**, 158 (1993).
- [8] M. G. Mayer and J. H. D. Jensen, *Elementary Theory of Nuclear Structure* (Wiley, New York, 1955).
- [9] B. D. Serot and J. D. Walecka, *Adv. Nucl. Phys.* **16**, 1 (1986).
- [10] M. M. Sharma, G. A. Lalazissis, and P. Ring, *Phys. Lett. B* **317**, 9 (1993).
- [11] M. M. Sharma *et al.*, *Phys. Rev. Lett.* **74**, 3744 (1994).
- [12] A. R. Bodmer, *Nucl. Phys. A* **526**, 703 (1991).
- [13] L. P. Gorkov, *Sov. Phys. JETP* **7**, 505 (1958).
- [14] H. Kucharek and P. Ring, *Z. Phys. A* **339**, 23 (1991).
- [15] M. M. Sharma, M. A. Nagarajan and P. Ring, *Phys. Lett. B* **312**, 377 (1993).
- [16] M. M. Sharma, in preparation (2000).
- [17] J. F. Berger *et al.*, *Nucl. Phys. A* **428**, 32 (1984).
- [18] G. Audi and A. H. Wapstra, *Nucl. Phys. A* **595**, 409 (1995).
- [19] J. Dobaczewski, H. Flocard and J. Treiner, *Nucl. Phys. A* **422**, 103 (1984).
- [20] Y. Aboussir *et al.*, *At. Data Nucl. Data Tables* **61**, 127 (1995).
- [21] J. M. Pearson *et al.*, *Phys. Lett. B* **387** 455 (1996).

- Fig. 1 The S_{2n} values for Zn isotopes in the waiting-point region with (a) NL-SH and NL-SV2 (b) NL-SV1 and HFB+SkP and (c) the mass formulae ETF-SI, and ETF-SI(Q) with shell quenching, as compared to the experimental data.
- Fig. 2 Evolution of the shell effects at $N = 82$ with the various forces for the isotopes chains of Mo, Zr, Sr and Kr in the vicinity of the neutron drip line.
- Fig. 3 (a) The neutron single-particle levels for Mo, Zr, Sr and Kr nuclei ($N=80$) near the neutron drip-line with the force NL-SV1. The Fermi energy is shown by the dashed lines. (b) The $N = 82$ shell gap in the neutron single-particle levels for ^{120}Zr with the various forces.

Fig. 1





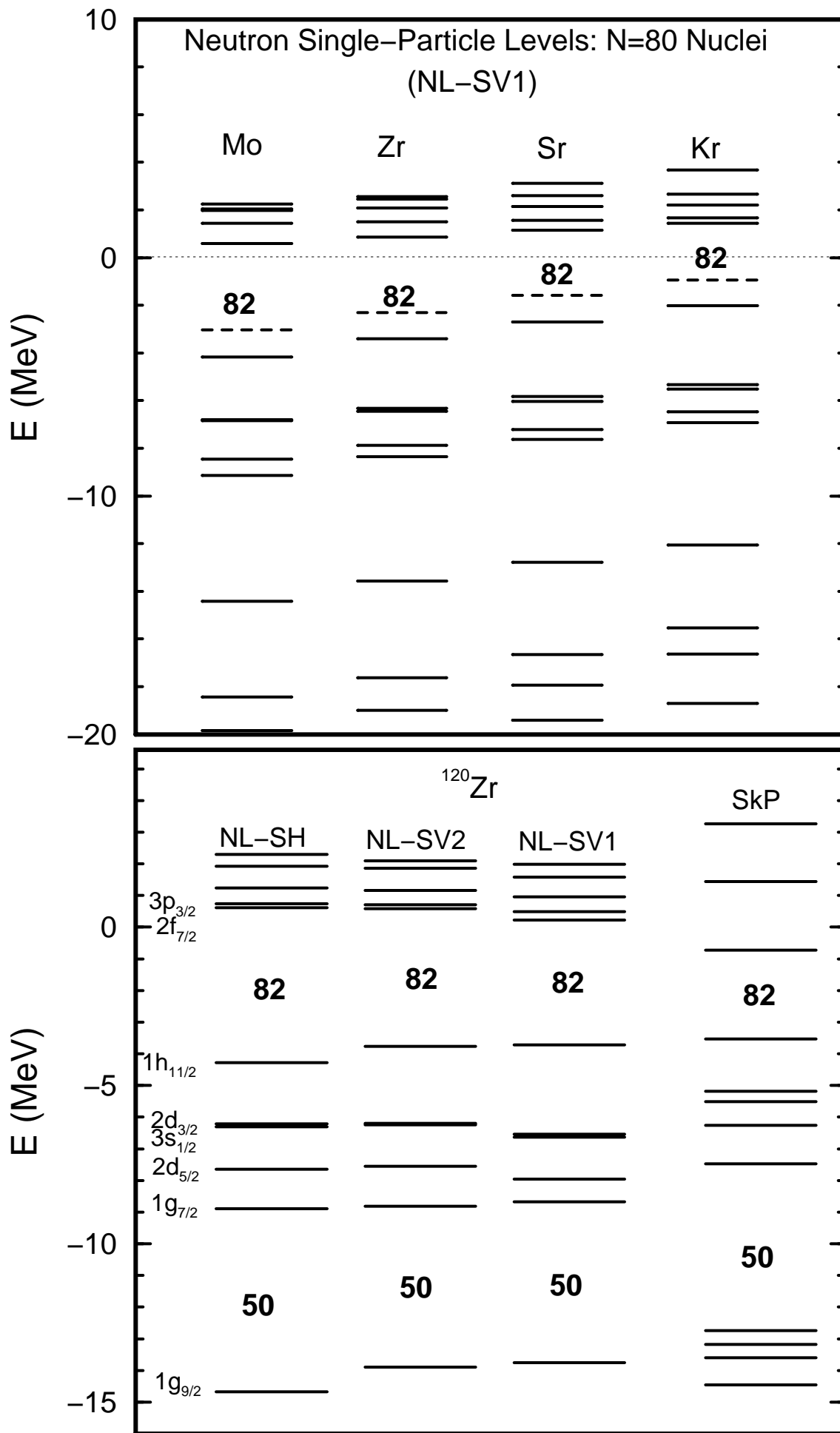


Fig. 3